Journal of Thermal Analysis and Calorimetry, Vol. 91 (2008) 3, 867–871

THE INFLUENCE OF MORPHOLOGY OF ULTRA-FINE CALCITE PARTICLES ON DECOMPOSITION KINETICS

Y.-L. Ren, X. Wang, M. Shui and R.-S. Li*

The State Key Laboratory Base of Novel Functional Materials and Preparation Science, Faculty of Materials Science and Chemical Engineering, Ningbo University, Ningbo 315211, China

The decomposition kinetics of reference calcite and three ultra-fine samples with different morphologies are investigated. The kinetic parameters and rate equation are obtained according to the methods reported in our previous studies. Compared with the reference calcite, a considerable diminution of the activation energy E_a up to 70–80 kJ mol^{-1} is observed in the case of three ultra-fine samples. There are also some distinct differences concerning the activation energy of each of the ultra-fine sample. This may have something to do with the particle morphology revealed by TEM and SEM measurements. XRD measurements of four calcite samples show that large strain exists in the crystal lattice in the case of ultra-fine calcite samples. This may give a reason to their abnormal decomposition behavior.

Keywords: *decomposition kinetics, ultra-fine calcite, Voigt analysis*

Introduction

Calcium carbonate is one of the most widely used fillers in many industrial applications such as plastics, rubber, papermaking and medicine. Recently it is found that the nano scale calcium carbonate has much more advantages over the commonly used normal sized calcium carbonate and its novel characteristics has attracted wide research interests.

As is known to all, constitutive phase of nano-material is ranging between molecular cluster and bulk substance. It may result in many special characteristics. For most of the nano-materials, blue shift and broadening of the absorption peaks will occur with the diminution of particle size [1, 2]. However, some nano-materials show both blue shift and red shift of the infra-red absorption peaks under the influence of the crystal expansion and hydrogen bonds [3]. An abnormal narrow ν_3 band together with a remarkable blue shift of about 40 cm^{-1} in the infra-red spectrum was observed in the report of Yue *et al.* [4]. They also found that the activation energy of the nano-crystalline calcium carbonate decreased dramatically by about 70–80 kJ mol^{-1} [5]. Of course, similar results were also reported by Criado, Ortega [6] and many other researchers. As is known that the thermal dynamics of calcium carbonate decomposition will vary with many factors such as the change of reaction condition, crystal form and particle size as a heterogeneous reaction system in that the heat transfer and mass transfer on the crystal boundaries is somewhat complex. Since that, although the dissociation of calcium carbonate has been widely studied and multiple techniques [7–10] were reported in literatures for determining the rate equation and deducing kinetic parameters, its rate equation and kinetic parameters reported in the literatures are still not well consistent [8, 10]. Usually, the literatures attribute the diminution of the activation energy to the larger surface energy stored on the surface of smaller particles or the size effect, but these ideas are just hypothesis and lack of experimental support.

In this paper, the thermal decomposition of ultra-fine calcite is studied according to the methods applied in our previous reports [5] to see the effect of particle size and morphology on the decomposition parameters and the rate equation. A preliminary explanation to the decrease of activation energy in the case of ultra-fine calcium carbonate is given based on the Voigt function analysis of XRD measurements from the viewpoint of lattice strain.

Experimental

Sample preparation

Purified CO_2 gas (20–40% concentration, diluted with N_2) bubbled through 5–10% $Ca(OH)_2$ until the pH was at 7–8. The precipitate was filtered, dried at 110°C to steady mass and then shifted through 320 mesh sieve. Under altered reaction conditions three ultra-fine calcite samples with different particle size and morphology were obtained, and referred to as 980227c, 980602 and 980622, respectively [11].

* Author for correspondence: shuimiao@nbu.edu.cn

1388–6150/$20.00

Akadémiai Kiadó, Budapest, Hungary
Springer, Dordrecht, The Netherlands

Characterization

All the thermal decomposition experiments were performed on a Shimadzu DT-30 thermal analyzer under the protection of nitrogen gas flow. The heating rates for both reference and the three ultra-fine samples were at 5, 10, 20, 50 K min^{-1}, respectively.

According to R_3 rate equation [5] determined by Kissinger [12] non-mechanical equation and master plot method [13], the decomposition kinetic parameters are obtained by Achar, Brindley and Sharp [14] equation

$$\ln\left[\frac{1}{f(\alpha)}\frac{\mathrm{d}\alpha}{\mathrm{d}T}\right]=\ln\left(\frac{A}{\beta}\right)+\frac{E_a}{RT} \quad (1)$$

and Coats and Redfern [15] equation

$$\log\left[\frac{g(\alpha)}{T^2}\right]=\log\left[\frac{AR}{E\beta}\right]-\frac{E_a}{2.303RT} \quad (2)$$

X-ray powder diffraction patterns were obtained at room temperature by a Philips diffractometer model X Pert MPD using CuK_α radiation at scanning step 0.02° and scanning rate 1° min^{-1}. PC-APD 4.0 software was used to separate K_{α_2} from K_{α_1} and Philips Profile Fit to obtain 2w and β. Calcite (99.99%, 5–20 μm estimated by SEM, Fig. 1) was used as reference sample without structural broadening. The apparent crystallite size or domain size D and the crystallite strain *e* are calculated according to the literatures [16, 17].

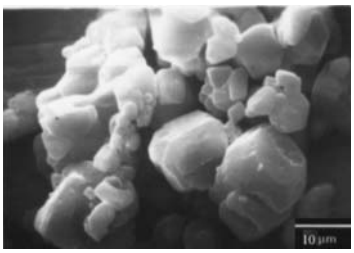

Fig. 1 The SEM image of reference calcite

Results and discussion

SEM or TEM images of ultra-fine calcite

TEM or SEM images of the three ultra-fine samples are shown as Figs 2a–c, consecutively. They show that sample 980227c has a cubic structure with the particle size estimated to be between 40 and 80 nm. Sample 980622 has a shuttle-form structure, about

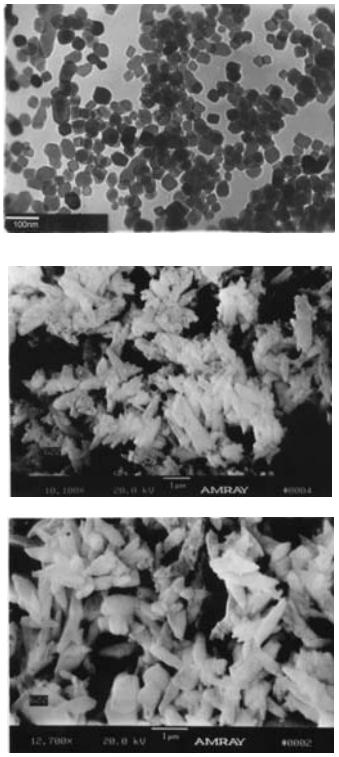

Fig. 2 The TEM or SEM for a – 980227c, b – 980602, c – 980622

1.5–2 μm long and 300–600 nm wide. The crystal lattices of both two samples seem integrated. There are also a few 100–400 nm cubic grains mixed with the shuttle-form particles in the case of 980622. Most of the particles in sample 980602 have loose shuttle-form structure, about 1–1.5 μm long and 200–600 nm wide. The sample also has a considerable number of 100–500 nm cubic grains. The sample with the structure shown in Fig. 2b seems to e in the process of the conglomeration of the base structure shown in Fig. 2a. Table 1 records the specific area of the reference calcite and three ultra-fine samples. The nano-crystalline calcite has the largest specific area because of its smaller particle size. The specific areas of three ultra-fine samples decrease in the sequence of 980227c, 980602 and 980622. The existence of agglomeration lessens the gap of specific surface area between ultra-fine samples and the reference calcite.

XRD measurements of ultra-fine calcite

The X-ray diffraction patterns of the reference calcite and three ultra-fine samples show that the intensity and the distance between crystal planes of diffraction

Table 1 The surface area of sample 980227c, 980602, 980622

Samples	980227c	980602	980622	Reference calcite
Specific area $S_g/m^2\ g^{-1}$	46.9	35.7	28.5	23.1

peaks are in good agreement with the standard spectrum of the crystalline polymorph calcite of calcium carbonate according to Mineral Powder Diffraction File Data Book, No. 5-586. The comparison assures us that the three samples are all calcite. Figure 3 shows the diffraction line profile of (110) plane for the three ultra-fine samples and the reference sample. Obviously, the diffraction line profiles of the three samples are broader than that of the reference calcite. The FWHM, integral breadth, crystallite size and lattice strain of (110), (113) and (202) plane for three ultra-fine samples are listed in Table 2.

The lattice strain in the case of three ultra-fine samples is about 1.2–1.8% and relatively large compared with the reference calcite. The lattice strain distribution is uniform not only in the different diffraction directions, but also between three ultra-fine samples. It seems that there is a kind of relationship between the particle size revealed by SEM or TEM images and the grain size on the different diffraction directions revealed by XRD measurements. The crystal grains of sample 980227c are cubic and the crystallite sizes on the different diffraction directions listed in Table 2 are close to each other, averaging 75 nm. Sample 980622 is consisted of shuttle-form particles and the crystallite sizes on the different diffraction directions vary. Sample 980602 has a loose shuttle-form structure. The variation of crystallite size on the different diffraction directions is in-between that of the other two ultra-fine samples. Shuttle-form particles that constitute sample 980622 seem as if they

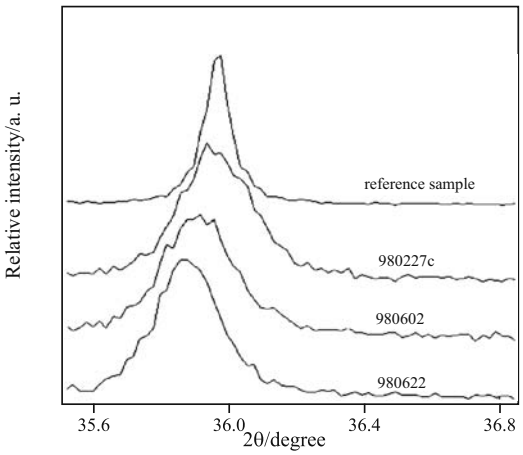

Fig. 3 X-ray diffraction intensity curve of (110) plane for reference calcite, sample 980227c, 980602 and 980622

are formed by crystal growth of the base structure showed in Fig 2a on the different crystal planes. The coexistence of loose shuttle-form structure and cubic grains shown in Fig. 2b to certain extent shows the process of conglomeration. The cell parameter *a* increases while *c* decreases with the formation of this agglomeration. We suggest that the force between the crystal interfaces of different directions may contribute to the variation of cell parameters.

Thermal decomposition of ultra-fine calcite

Figure 4 shows the TG, DTA and DTG curves of the reference calcite and three ultra-fine samples at the heat-

Table 2 The experimental data of (110), (113), (202) plane X-ray diffraction for three samples and the results of Voigt function analysis

		reference calcite	980227c	980602	980622
110 plane diffraction	2θ/°	35.955	35.914	35.869	35.841
	2ω/°	0.077	0.212	0.216	0.182
	β/°	0.109	0.289	0.292	0.243
	$e \cdot 10^3$	<0.1	1.7	1.8	1.6
	D/nm	>1000	77.8	79.9	123.5
113 plane diffraction	2θ/°	39.390	39.364	39.320	39.279
	2ω/°	0.078	0.217	0.195	0.200
	β/°	0.109	0.297	0.278	0.278
	$e \cdot 10^3$	<0.1	1.6	1.2	1.4
	D/nm	>1000	71.8	55.0	74.2
202 plane diffraction	2θ/°	43.145	43.097	43.047	43.018
	2ω/°	0.079	0.210	0.228	0.193
	β/°	0.104	0.283	0.319	0.268
	$e \cdot 10^3$	<0.1	1.4	1.3	1.1
	D/nm	>1000	73.8	52.8	69.7
Cell parameter	*a*/Å	4.9908	5.0013	5.0074	5.0103
	c/Å	17.062	16.7906	16.7800	16.7765

Table 3 The activation energy for samples 980602, 980622, 980227c and reference calcite at the heating rate of 5, 10, 20, 50 K min^{-1}

Heating rate/ K min^{-1}	980227c E_a/kJ mol^{-1}		980602 E_a/kJ mol^{-1}		980622 E_a/kJ mol^{-1}		Reference calcite E_a/kJ mol^{-1}	
	differential	integral	differential	integral	differential	integral	differential	integral
5	124.2±2.5	128.2±3.0	135.8±2.7	140.6±3.3	142.5±2.8	147.6±3.5	204.8±4.1	208.4±4.8
10	120.3±3.2	125.6±3.2	136.8±3.6	141.3±3.6	141.3±3.8	145.3±3.7	204.1±5.4	206.3±5.2
20	117.8±3.5	126.3±3.7	130.9±3.9	135.6±4.0	139.9±4.2	140.3±4.1	199.8±5.9	200.7±5.9
50	117.2±4.6	120.6±4.3	128.6±5.0	132.2±4.7	140.2±5.5	140.2±5.0	197.2±7.7	201.5±7.2
Average E_a	120.0±3.5	125.2±3.6	133.0±3.8	137.4±3.9	141.0±4.1	143.4±4.1	201.5±5.8	204.±5.8

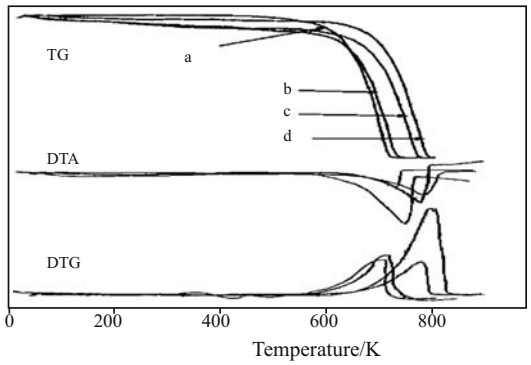

Fig. 4 TG, DTA and DTG curves for a – 980227c, b – 980602, c – 980622, d – reference calcite at the heating rate of 10 K min^{-1}

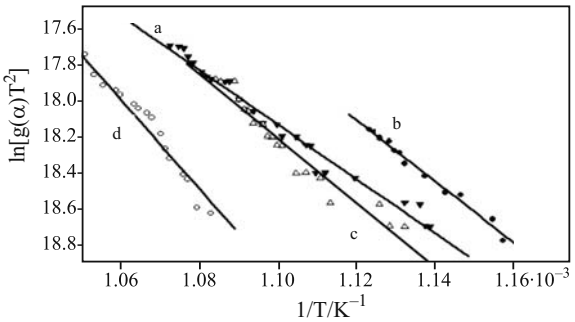

Fig. 5 $\ln[g(\alpha)/T^2]$ *vs.* $1/T$ for a – 980227c, b – 980602, c – 980622, d – reference calcite at the heating rate of 10 K min^{-1}

ing rate of 10 K min^{-1}. The TG curve of the sample 980227c seems steep and exhibits lower decomposition temperature while that of the reference calcite behaves otherwise. The TG curves shift toward the high temperature area at the sequence of 980227c, 980602, 980622 and the reference calcite. The DTA and DTG curves of the samples have the similar shift tendency.

The rate equation is determined to be R_3 on the basis of the set of method previously reported [5]. Then according to Eq. (1) and Eq. (2), plot $\ln[g(\alpha)/T^2]$ referred to as integral method and $\ln\{d\alpha/[f(\alpha)dT]\}$ referred to as differential method *vs.* $1/T$, respectively. The activation energies of the reference calcite and three ultra-fine samples are obtained and listed in Table 3. Figure 5 shows the plot of $\ln[g(\alpha)/T^2]$ *vs.* $1/T$.

The activation energy of the tested sample increases slightly with the decrease of the heating rate. The results obtained by differential method and integral method are basically the same. Compared with the reference calcite, the three ultra-fine samples exhibit a diminution of activation energy up to 60–80 kJ mol^{-1} and the activation energies of three ultra-fine samples decrease at the sequence of 980622, 980602 and 980227c, which is consistent with their degree of agglomeration. The difference of activation energy for three ultra-fine samples is at the order of 6–12 kJ mol^{-1}.

The specific areas of the reference calcite and three ultra-fine samples show that the large diminution in activation energy of ultra-fine samples cannot be solely explained by the larger surface energy that smaller particles have. XRD measurements reveal that large strain exists in the lattice of the ultra-fine samples. It may lower the integrity of crystal lattice and further contribute to the obvious diminution in activation energy. As to the distinct differences among three ultra-fine samples, the variation of specific area and surface energy and the existence of force field at the grain interface with the formation of agglomeration may be the reason.

Conclusions

TEM or SEM images reveal the microstructures of the reference calcite and three ultra-fine samples synthesized by altered reaction conditions. The three ultra-fine samples have the similar grain size calculated by XRD measurements but different particle morphology. The degree of agglomeration increases at the sequence of 980227c, 980602 and 980622. A considerable diminution of the activation energy E_a up to 70–80 kJ mol^{-1} is observed by TG experiments of those samples in the case of three ultra-fine samples compared with the reference calcite. Also, distinct differences in activation energy about 6–12 kJ mol^{-1} exist among the three ultra-fine samples. We suggest that the large lattice strain

revealed by XRD measurements may contribute to the abnormal activation energy diminution. The variation of specific area, surface energy and the existence of force field at the grain interface with the formation of agglomeration may be the reason of slight differences between the three ultra-fine samples.

Acknowledgements

We greatfully acknowledge support for this work from Ningbo Science and Technology Bureau project 2006B100064.

References

1 P. Ball and L. Garwin, Nature, 355 (1992) 761.
2 L. D. Zhang and J. M. Mou, Science of Nanomaterial, Liaoning Sci. Pub., 1994, p. 30.
3 X. S.Ye and J. Sha, Function Mater., 29 (1998) 287.
4 L. H. Yue, M. Shui and Z. D. Xu, Spectrosc. Lett., 34 (2001) 793.
5 L. H. Yue, M. Shui and Z. D. Xu, Thermochim. Acta, 335 (1999) 121.
6 J. M. Criado and A. Ortega, Thermochim. Acta, 195 (1992) 163.
7 R. T. Rajeswara, Chem. Eng. Technol., 19 (1996) 373.
8 J. M. Criado, J. Malek and A. Ortega, Thermochim. Acta, 147 (1989) 377.
9 J. Malek, Thermochim. Acta, 200 (1992) 257.
10 A. M. Gadalla, Thermochim. Acta, 95 (1985) 179.
11 J. X. Cai and L. H. Yue, Inorg. Salt Industry, 5 (1995) 7.
12 H. E. Kissinger, J. Res. Natl. Bur. Stand., 57 (1956) 712.
13 J. Malek, Thermochim. Acta, 200 (1992) 257.
14 J. H. Sharp and S. A. Wendworth, Anal. Chem., 41 (1969) 2060.
15 A. W. Coats and J. P. Redfern, Nature, 201 (1964) 68.
16 T. H. de Keijser, J. I. Langford, E. J. Mittemeijer and A. B. P. Vogels, J. Appl. Crystallogr., 15 (1982) 308.
17 J. I. Langford, J. Appl. Crystallogr., 11 (1978) 10.

Received: June 16, 2007
Accepted: July 11, 2007

DOI: 10.1007/s10973-007-8610-x